Computational Materials Science 120 (2016) 77–83

Contents lists available at ScienceDirect

Computational Materials Science

journal homepage: www.elsevier.com/locate/commatsci

Extended higher-order multi-phase-field model for three-dimensional anisotropic-grain-growth simulations

Eisuke Miyoshi [a], Tomohiro Takaki [b,*]

[a] Department of Mechanical and System Engineering, Kyoto Institute of Technology, Matsugasaki, Sakyo, Kyoto 606-8585, Japan
[b] Faculty of Mechanical Engineering, Kyoto Institute of Technology, Matsugasaki, Sakyo, Kyoto 606-8585, Japan

ARTICLE INFO

Article history:
Received 10 February 2016
Received in revised form 8 April 2016
Accepted 10 April 2016
Available online 26 April 2016

Keywords:
Multi-phase-field model
Grain growth
Anisotropic grain-boundary energy
Anisotropic grain-boundary mobility
Quadruple junction

ABSTRACT

Based on the multi-phase-field (MPF) model reported by Steinbach et al., we constructed a higher-order MPF model in a previous study that contains a higher-order term and an additional kinetic parameter to represent the properties of triple junctions (TJs); this model was observed to be suitable for the simulation of 2D grain growth with anisotropic grain-boundary (GB) energy and mobility, which are strongly dependent on the misorientation angle ($\Delta\theta$). In the current study, we attempt to improve the accuracy of 3D MPF simulations of anisotropic grain growth by extending this higher-order MPF model such that it accounts for the properties of quadruple junctions as well as those of TJs. In addition, using the extended higher-order MPF model, a series of grain-growth simulations are performed for a 3D columnar structure while considering the anisotropic GB properties, through which the accuracy of the model is examined in detail. The results confirm that the extended higher-order MPF model enables the anisotropic GB properties to be handled accurately for wider-ranging $\Delta\theta$ than in previous models.

1. Introduction

During the heat treatment of a polycrystalline material, the internal microstructure evolves through several thermodynamic phenomena including multiple phase transformations, recrystallization, and grain growth [1–3]. Control over the microstructural evolution enables superior materials to be produced because the physical and mechanical properties of polycrystals are greatly dependent on the microstructure. In general, the fundamental process underlying the microstructural evolution is the migration of grain boundaries (GBs), or grain growth in a broad sense. Thus, with the aim of systematically predicting the evolution of microstructure with heat treatment, numerical approaches have been developed using mesoscale grain-growth models including the Monte-Carlo model [4–7], cellular automaton model [8–10], vertex model [11–14], surface-evolver model [15], front-tracking model [16–18], level-set model [19,20], and phase-field model [21–25].

Recently, the multi-phase-field (MPF) model proposed by Steinbach et al. [26,27] has been frequently used as a prominent model to simulate polycrystalline grain growth. This model enables the quantitative prediction of complicated microstructural evolution in time and space. Additionally, the computation speed of the model can be significantly increased by using the active parameter tracking algorithm [28–30] that was proposed by Vedantam and Patnaik [28], Gruber et al. [31], and Kim et al. [32] independently. However, the original MPF model has one drawback: in real materials, the properties (energy and mobility) of GBs exhibit strong anisotropies, with their variations depending primarily on the misorientation angle ($\Delta\theta$) between the neighboring grains [1,33–36]. These anisotropic properties affect both the kinetics and morphological aspects of grain growth [36–40] and, thus, might be important factors to consider in grain-growth simulations. However, it is difficult to introduce the anisotropic properties in the MPF model for wide-ranging $\Delta\theta$ because when GB properties with large differences are introduced in MPF simulations, unnecessary phases ('ghost phases [41]') leak from multiple junctions into GBs, and consequently, the GB behaviors become unstable. To address this issue, Garcke et al. [42,43] and Hirouchi et al. [44] have proposed modified models, which are known as higher-order MPF models. In these models, the formation of ghost phases is suppressed using a higher-order term representing the free energy of triple junctions (TJs). However, the coefficient of the higher-order term used for the models, which strongly affects the simulation results, has not been optimized. Moreover, the models do not account for the decrease in the accuracy due to the strong anisotropy in GB mobility. Therefore, we developed a novel

* Corresponding author. Tel./fax: +81 75 724 7317.
E-mail address: takaki@kit.ac.jp (T. Takaki).

http://dx.doi.org/10.1016/j.commatsci.2016.04.014
0927-0256/

higher-order MPF model [45] by optimizing the coefficient of the higher-order term and introducing the TJ mobility; the validity of the model was confirmed via a series of 2D grain-growth simulations with anisotropic GB properties. However, 3D simulations are essential for simulating actual grain growth [32,33,46], on which quadruple junctions (QJs) as well as TJs might have a considerable effect [33]. Recently, 3D MPF simulation is becoming easy to perform by virtue of parallel computing [47–49] and general-purpose computing on graphics processing units (GPUs) [50–57]. Thus, the improvement of the accuracy of 3D MPF simulation is believed to be an urgent issue.

In this study, we attempt to improve the accuracy of 3D grain-growth simulations with anisotropic GB properties by introducing the properties of QJs to the higher-order MPF model that was proposed in our previous study [45]. First, in Section 2, the higher-order MPF model is extended to account for the QJ properties. Next, in Section 3, the appropriate ways to determine the simulation parameters used for the extended higher-order model are examined. Finally, in the same section, the accuracy of the extended model using the determined parameters is tested using grain-growth simulations with $\Delta\theta$-dependent GB properties.

2. Extended higher-order MPF model considering QJ properties

We derive the governing equation of the extended higher-order MPF model that accounts for the QJ properties. The MPF model represents a polycrystalline system consisting of N grains using N phase-field variables; the ith grain is represented by the phase field ϕ_i, which takes a value of 1 in the ith grain, 0 in the other grains, and $0 < \phi_i < 1$ at the GBs. The sum of the phase fields at any spatial point in the system must be conserved:

$$\sum_{i=1}^{n}\phi_i = 1, \tag{1}$$

where n is the number of coexisting phases at the point.

When the additional free energy of the TJs and QJs are considered, the total free energy of the system can be expressed as

$$F = \int_V \sum_{i=1}^{n}\sum_{j=i+1}^{n}\left\{W_{ij}\phi_i\phi_j + \sum_{k=j+1}^{n}(W_{ijk}\phi_i\phi_j\phi_k + \sum_{l=k+1}^{n}W_{ijkl}\phi_i\phi_j\phi_k\phi_l) - \frac{a_{ij}^2}{2}\nabla\phi_i\cdot\nabla\phi_j\right\}\mathrm{d}V, \tag{2}$$

where W_{ij} and a_{ij} are the barrier height and gradient coefficient of the GB between the ith and jth grains, respectively. The second and third terms on the right-hand side in Eq. (2) are the higher-order terms representing the energetic contributions of the TJs [42–44,58,59] and QJs, respectively. These terms play a role in penalizing ghost phases at the GBs around the junctions. The coefficients W_{ijk} and W_{ijkl} are the barrier heights of TJs and QJs, respectively. A suitable way of determining W_{ijkl} is examined in Section 3; W_{ijk} is expressed by the formula developed in our previous study [45]:

$$W_{ijk} = \begin{cases} k_{\mathrm{TJ}}\left(W_{\mathrm{GB,max}} - \frac{W_{\mathrm{GB,median}}+W_{\mathrm{GB,min}}}{2}\right) & \text{for } 2W_{\mathrm{GB,median}} \leqslant W_{\mathrm{GB,max}} + W_{\mathrm{GB,min}}, \\ 0 & \text{for } 2W_{\mathrm{GB,median}} > W_{\mathrm{GB,max}} + W_{\mathrm{GB,min}}, \end{cases} \tag{3}$$

where $W_{\mathrm{GB,max}}$, $W_{\mathrm{GB,median}}$, and $W_{\mathrm{GB,min}}$ are the maximum, median, and minimum barrier heights of the GBs adjoining the TJ, respectively, and k_{TJ} is a constant. The optimum value of k_{TJ} for 3D simulations is examined in Section 3.

The time-evolution equation for ϕ_i satisfying Eq. (1) is given by

$$\frac{\partial\phi_i}{\partial t} = -\frac{2}{n}\sum_{j=1}^{n}M_{ij}^{\phi}\left(\frac{\delta F}{\delta\phi_i} - \frac{\delta F}{\delta\phi_j}\right), \tag{4}$$

where M_{ij}^{ϕ} is the phase-field mobility of the GB between the ith and jth grains. The functional derivative of Eq. (2) can be calculated as

$$\frac{\delta F}{\delta\phi_i} = \sum_{k=1}^{n}\left\{W_{ik}\phi_k + \sum_{l=1}^{n}\left(W_{ikl}\phi_k\phi_l + \sum_{m=1}^{n}W_{iklm}\phi_k\phi_l\phi_m\right) + \frac{a_{ik}^2}{2}\nabla^2\phi_k\right\}. \tag{5}$$

Finally, the time-evolution equation reduces to

$$\frac{\partial\phi_i}{\partial t} = -\frac{2}{n}\sum_{j=1}^{n}M_{ij}^{\phi}\sum_{k=1}^{n}\left[\frac{1}{2}(a_{ik}^2 - a_{jk}^2)\nabla^2\phi_k + (W_{ik} - W_{jk})\phi_k + \sum_{l=1}^{n}\left\{(W_{ikl} - W_{jkl})\phi_k\phi_l + \sum_{m=1}^{n}(W_{iklm} - W_{jklm})\phi_k\phi_l\phi_m\right\}\right]. \tag{6}$$

W_{ij}, a_{ij}, and M_{ij}^{ϕ} can be related to the thickness (δ), energy (γ_{ij}), and mobility (M_{ij}) of the GB through the following equations:

$$W_{ij} = \frac{4\gamma_{ij}}{\delta}, \quad a_{ij} = \frac{2}{\pi}\sqrt{2\delta\gamma_{ij}}, \quad M_{ij}^{\phi} = \frac{\pi^2}{8\delta}M_{ij}. \tag{7}$$

When M_{ij}^{ϕ} defined in Eq. (7) is substituted into Eq. (6), the migration of the TJ, ijk, is determined by the linear superposition of the GB mobilities, M_{ij}, M_{jk}, and M_{ki}. Thus, when one of the mobilities in the TJ is much higher or lower than the others, it dominates the migration of the TJ, resulting in the occurrence of artificial junction drag on the GBs. To avoid this issue, we modify the definition of M_{ij}^{ϕ} in TJs ($n = 3$) as follows by introducing the TJ mobility M_{ijk} [45]:

$$\left.\begin{aligned} M_{ij}^{\phi} = M_{jk}^{\phi} = M_{ki}^{\phi} &= \tfrac{\pi^2}{8\delta}M_{ijk} \\ M_{ijk} &= M_{ij}\omega_{ij} + M_{jk}\omega_{jk} + M_{ki}\omega_{ki} \end{aligned}\right\} \text{only for } n = 3, \tag{8}$$

where ω_{ij} is the weight function defined as follows using a constant m_{TJ} and the average of the GB mobilities $M_{\mathrm{GB,ave}} = (M_{ij} + M_{jk} + M_{ki})/3$:

$$\omega_{ij} = \frac{1}{2}\left(1 - \frac{|M_{ij} - M_{\mathrm{GB,ave}}|^{m_{\mathrm{TJ}}}}{|M_{ij} - M_{\mathrm{GB,ave}}|^{m_{\mathrm{TJ}}} + |M_{jk} - M_{\mathrm{GB,ave}}|^{m_{\mathrm{TJ}}} + |M_{ki} - M_{\mathrm{GB,ave}}|^{m_{\mathrm{TJ}}}}\right). \tag{9}$$

m_{TJ} represents the strength of the weighting; when m_{TJ} is set to zero, M_{ijk} is equal to $M_{\mathrm{GB,ave}}$. Further, to accurately express the QJ behaviors, the QJ mobility, M_{ijkl}, is introduced by extending the formulation of M_{ijk} as follows:

$$\left.\begin{aligned} M_{ij}^{\phi} = M_{jk}^{\phi} = M_{kl}^{\phi} = M_{li}^{\phi} &= \tfrac{\pi^2}{8\delta}M_{ijkl} \\ M_{ijkl} &= M_{ijk}\omega_{ijk} + M_{jkl}\omega_{jkl} + M_{kli}\omega_{kli} + M_{lij}\omega_{lij} \end{aligned}\right\} \text{only for } n = 4, \tag{10}$$

$$\omega_{ijk} = \frac{1}{3}\left(1 - \frac{|M_{ijk} - M_{\mathrm{TJ,ave}}|^{m_{\mathrm{QJ}}}}{|M_{ijk} - M_{\mathrm{TJ,ave}}|^{m_{\mathrm{QJ}}} + |M_{jkl} - M_{\mathrm{TJ,ave}}|^{m_{\mathrm{QJ}}} + |M_{kli} - M_{\mathrm{TJ,ave}}|^{m_{\mathrm{QJ}}} + |M_{lij} - M_{\mathrm{TJ,ave}}|^{m_{\mathrm{QJ}}}}\right), \tag{11}$$

where m_{QJ} is a constant and $M_{\mathrm{TJ,ave}} = (M_{ijk} + M_{jkl} + M_{kli} + M_{lij})/4$ is the average of the TJ mobilities. The optimum values of m_{TJ} and m_{QJ} for 3D simulations are determined in Section 3.

3. Determination of the parameters and their validations

3.1. Coefficients of the higher-order terms: W_{ijk} and W_{ijkl}

We examine the optimum values of the coefficients of the higher-order terms in Eq. (6), W_{ijk} and W_{ijkl}, for 3D problems, by evaluating the accuracy of the extended higher-order MPF model. As the simulation model, we employ a simple 3D system, illustrated in Fig. 1, that contains TJs and QJs; the steady-state boundary velocity, V, is compared with the theoretical value. The domain

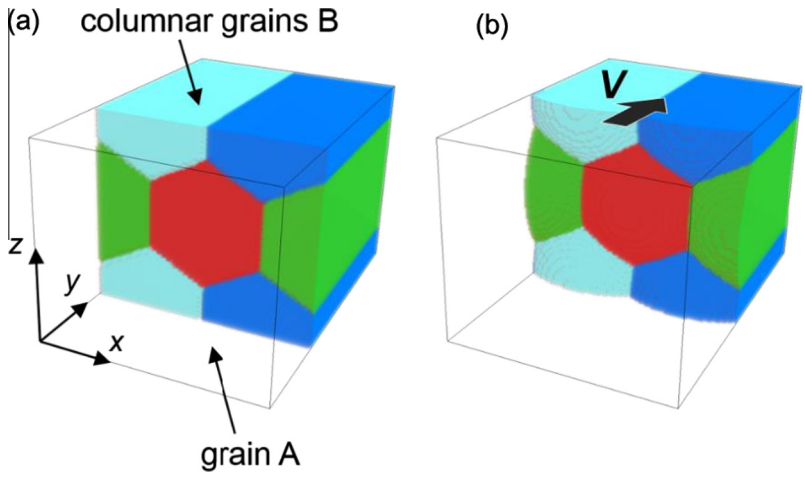

Fig. 1. Simulation models used to evaluate the accuracy of the extended higher-order MPF model for anisotropic grain growth: (a) initial state and (b) steady state.

is divided into a grid of 88 × 128 × 76 regular square lattices with a size of Δx = 1 μm. The system consists of a coarse grain A and the assembly of columnar grains B that are under periodic boundary conditions in the x- and z-directions and zero-flux condition in the y-direction. The cross sections of the columnar grains are regular hexagons with a size of $a = 25\Delta x$ on each side. The theoretical value of V, V_{th}, is given by [1]

$$V_{th} = M_{AB}E_B, \tag{12}$$

where M_{AB} is the mobility of the GBs between the grain A and columnar grains B; E_B is the GB energy per unit volume in the assembly of the grains B. E_B can be calculated geometrically:

$$E_B = \frac{2\gamma_{BB}}{\sqrt{3}a}, \tag{13}$$

where γ_{BB} is the energy of the GB between the grains B. In the following simulations, the energy of the A–B boundaries, γ_{AB}, and the mobility of the B–B boundaries, M_{BB}, are fixed to 1 J/m^2 and 1 m^4/(J s), respectively. However, γ_{BB} and M_{AB} are varied. The time increment Δt is taken as large as possible such that it satisfies the stability condition of the explicit scheme. Here, we developed our own CUDA C code to accelerate MPF simulations by single-GPU (NVIDIA Tesla K80) computing, which was observed to improve the computation speed by a factor of 20 compared with that of single-CPU (Intel Xeon E5-2697) computing. The GPU acceleration enabled us to perform systematic simulations of thousands of times that were required in this study.

In general, in addition to the grid resolution, the accuracy of the MPF simulation is affected by the GB thickness, δ, because of the diffuse nature of the phase-field model. Therefore, to determine the suitable setting of δ for evaluating the accuracy of the extended higher-order model, we first performed simulations while varying δ, through which the variation of the relative error $(V - V_{th})/V_{th}$ was determined. Note that the grid resolution remained the same as that described above (88 × 128 × 76 grids) for the convenience of computational costs. The simulation results are presented in Fig. 2. Here, the conditions $\gamma_{BB} = \gamma_{AB}$ and $M_{AB} = M_{BB}$ were employed. Fig. 2 shows that $\delta = 3\Delta x$ yields an error larger than 10%. In addition, when $\delta \geqslant 5\Delta x$, accurate results are not obtained, and thus, these δ are considered too large compared with the grid resolution of the system. In contrast, the result obtained for $\delta = 4\Delta x$ exhibits good agreement with the theory with an error of less than 0.1%. Thus, we used $\delta = 4\Delta x$ for the simulations that follow.

Next, we performed simulations using the above-described conditions while varying the energy ratio γ_{BB}/γ_{AB}, with $M_{AB} = M_{BB}$. Note

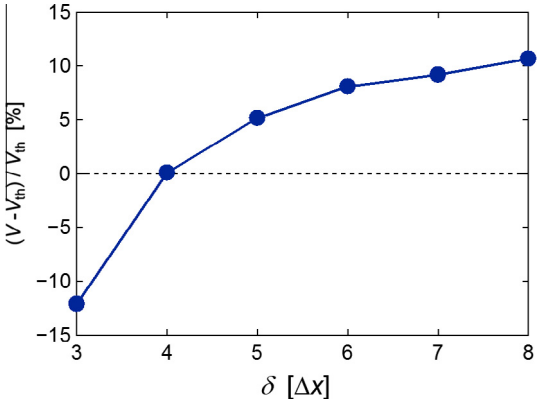

Fig. 2. Variation of $(V - V_{th})/V_{th}$ as a function of δ for the simulations with $\gamma_{BB} = \gamma_{AB}$ and $M_{AB} = M_{BB}$.

that when $\gamma_{BB}/\gamma_{AB} \geqslant \sqrt{3}$, QJs disappear because of the occurrence of solid-state wetting [60–62]. Therefore, we limited γ_{BB} such that $\gamma_{BB}/\gamma_{AB} < \sqrt{3}$. The value of k_{TJ} in Eq. (3) was set to 0, 1, 2, 3, and 4. Further, for each γ_{BB}/γ_{AB} and each k_{TJ}, the value of W_{ijkl} in Eq. (6) was varied by 0.1 MJ/m^3, through which the variations of the relative error $(V - V_{th})/V_{th}$ were determined. Here, W_{ijkl} was limited to zero or positive values because setting W_{ijkl} to a negative value causes the free energy of the QJ to become lower than that of the

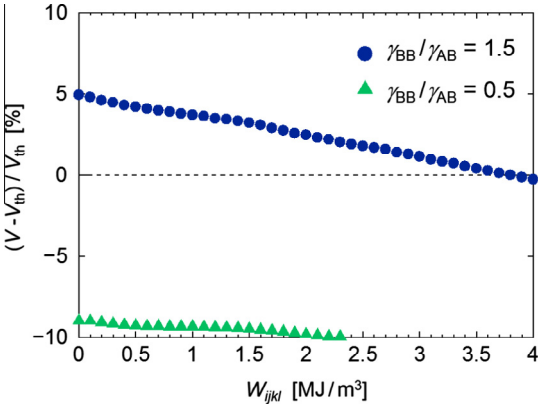

Fig. 3. Variation of $(V - V_{th})/V_{th}$ as a function of W_{ijkl} for the simulations of γ_{BB}/γ_{AB} = 0.5 and 1.5 with k_{TJ} = 4.

GBs, and consequently, the GBs become unstable. As examples, Fig. 3 presents the simulation results obtained for $\gamma_{BB}/\gamma_{AB} = 0.5$ and 1.5 with $k_{TJ} = 4$. The results indicate that in both cases, as W_{ijkl} increases, $(V - V_{th})/V_{th}$ decreases almost monotonically. For $\gamma_{BB}/\gamma_{AB} = 1.5$, the magnitude of the relative error, $|(V - V_{th})/V_{th}|$, becomes approximately zero at $W_{ijkl} = 3.8$ MJ/m^3. However, for $\gamma_{BB}/\gamma_{AB} = 0.5$, $|(V - V_{th})/V_{th}|$ does not become zero, reaching its minimum value at $W_{ijkl} = 0$ MJ/m^3. These values of W_{ijkl}, which minimize $|(V - V_{th})/V_{th}|$, are defined as the optimum values. The optimum values of W_{ijkl} for each γ_{BB}/γ_{AB} and each k_{TJ} are presented in Fig. 4(a). In addition, Fig. 4(b) shows the variations of $(V - V_{th})/V_{th}$ obtained using the extended higher-order model with the optimum W_{ijkl} value in Fig. 4(a). Fig. 4(a) shows that for $\gamma_{BB}/\gamma_{AB} < 1$, the optimum W_{ijkl} is zero for every case, suggesting that the higher-order terms do not work effectively. However, for $0.3 \leqslant \gamma_{BB}/\gamma_{AB} < 1$, relatively stable simulation is possible with an error of less than 10%, as demonstrated in Fig. 4(b). For $\gamma_{BB}/\gamma_{AB} < 0.3$, $(V - V_{th})/V_{th}$ jumps sharply to the positive side. In this range, significant leakage of ghost phases into the GBs occurs for every value of W_{ijkl}. In contrast, for $\gamma_{BB}/\gamma_{AB} \geqslant 1$, $(V - V_{th})/V_{th}$ can be suppressed to zero using the optimum W_{ijkl} value, excluding the case of $k_{TJ} = 4$ for $\gamma_{BB}/\gamma_{AB} = 1.7$.

The aforementioned results indicate that for $\gamma_{BB}/\gamma_{AB} \geqslant 1$, the higher-order terms significantly improve the accuracy of the 3D MPF simulations using k_{TJ} values less than 4 and the corresponding W_{ijkl} value in Fig. 4(a). Therefore, this study employs $k_{TJ} = 3$ because this value also yields relatively accurate results in 2D simulations [45]. Further, we created the following formula as an approximate function of the optimum W_{ijkl} value in Fig. 4(a) for $k_{TJ} = 3$:

$$W_{ijkl} = k_{QJ}(W_{TJ,ave} - W_{TJ,min}) \times \left(\frac{W_{GB,min}}{W_{GB,max}}\right)^{p}, \quad (14)$$

where k_{QJ} and p are the fitting parameters; $W_{TJ,ave}$ and $W_{TJ,min}$ are the average and minimum barrier heights of TJs adjoining the QJ, respectively; and $W_{GB,max}$ and $W_{GB,min}$ are the maximum and minimum barrier heights of the GBs adjoining the QJ, respectively. The curve for Eq. (14) with $k_{QJ} = 113$ and $p = 4$ is shown in Fig. 4(a) as a solid line, from which we can confirm that Eq. (14) fits the data well for $k_{TJ} = 3$.

To validate the extended higher-order MPF model with W_{ijk} (Eq. (3) with $k_{TJ} = 3$) and W_{ijkl} (Eq. (14) with $k_{QJ} = 113$ and $p = 4$), we performed additional simulations in the same manner as stated above. For comparison, the original model without higher-order terms and the higher-order model with only W_{ijk} (Eq. (3) with $k_{TJ} = 3$) were also employed. Fig. 5 presents the simulation results. Here, the results for $\gamma_{BB}/\gamma_{AB} < 1$ are omitted because $W_{ijk} = W_{ijkl} = 0$ in this range, and all the results are the same. In Fig. 5, the errors

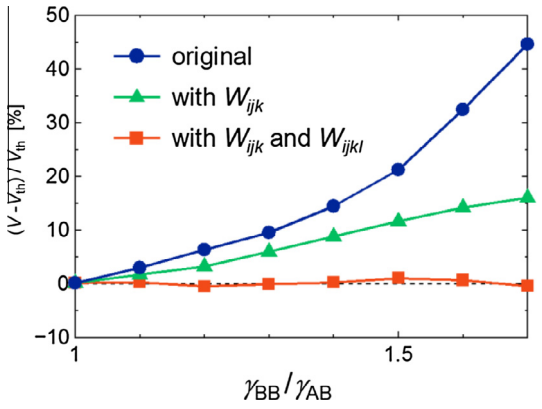

Fig. 5. Variation of $(V - V_{th})/V_{th}$ as a function of γ_{BB}/γ_{AB} obtained using three MPF models: the original model without higher-order terms, higher-order model with only W_{ijk}, and extended higher-order model with W_{ijk} and W_{ijkl}.

$(V - V_{th})/V_{th}$ determined using the original model and the higher-order model with only W_{ijk} increase monotonically with increasing γ_{BB}/γ_{AB}, becoming larger than 10%. However, the error of the extended model is at most 1%, and the accuracy is notably high. These findings indicate that the extended model is effective in accurately simulating 3D grain growth with anisotropic GB properties.

3.2. Multiple-junction mobilities: M_{ijk} and M_{ijkl}

To determine the suitable settings of the exponents m_{TJ} in Eq. (9) and m_{QJ} in Eq. (11), we performed simulations using the system shown in Fig. 1 and determined the relative error $(V - V_{th})/V_{th}$ for various values of M_{AB}/M_{BB}, with γ_{BB}/γ_{AB} fixed to 1. Here, m_{TJ} and m_{QJ} were set to 0, 10, and 20. Fig. 6 plots the variation of $(V - V_{th})/V_{th}$ as a function of M_{AB}/M_{BB}. Fig. 6(a) reveals that the magnitude of the error for $m_{TJ} = 0$ increases as M_{AB}/M_{BB} deviates from 1, irrespective of the value of m_{QJ}. The decrease in the accuracy is notable especially for the range $M_{AB}/M_{BB} < 1$, in which the error exceeds 20% at $M_{AB}/M_{BB} = 0.01$. However, as observed in Fig. 6(b) and (c), increasing m_{TJ} results in a smaller error. In particular, using $m_{TJ} = 20$ and a non-zero value of m_{QJ}, the magnitude of the error is less than approximately 0.1% over $0.01 \leqslant M_{AB}/M_{BB} \leqslant 100$, and the accuracy is notably high. Note that when increasing m_{TJ} and m_{QJ} to values larger than 20, there is almost no change in the result. Additionally, too large of values of m_{TJ} and m_{QJ} can lead to arithmetic overflows or underflows in the exponential operations for Eqs. (9) and (11). Therefore, we employed $m_{TJ} = m_{QJ} = 20$ for the remainder of the study.

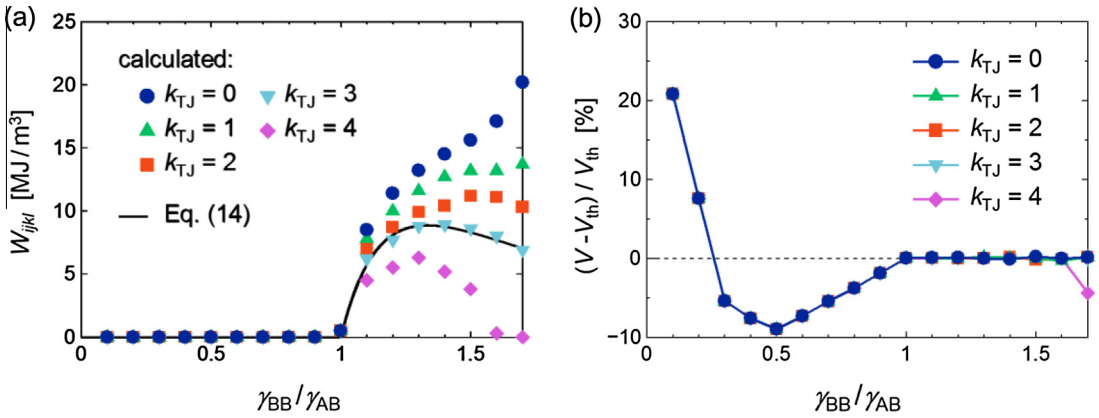

Fig. 4. (a) Variation of the optimum value of W_{ijkl} to minimize $|(V - V_{th})/V_{th}|$ as a function of γ_{BB}/γ_{AB} for various k_{TJ} values; (b) $(V - V_{th})/V_{th}$ calculated using the W_{ijkl} values shown in (a).

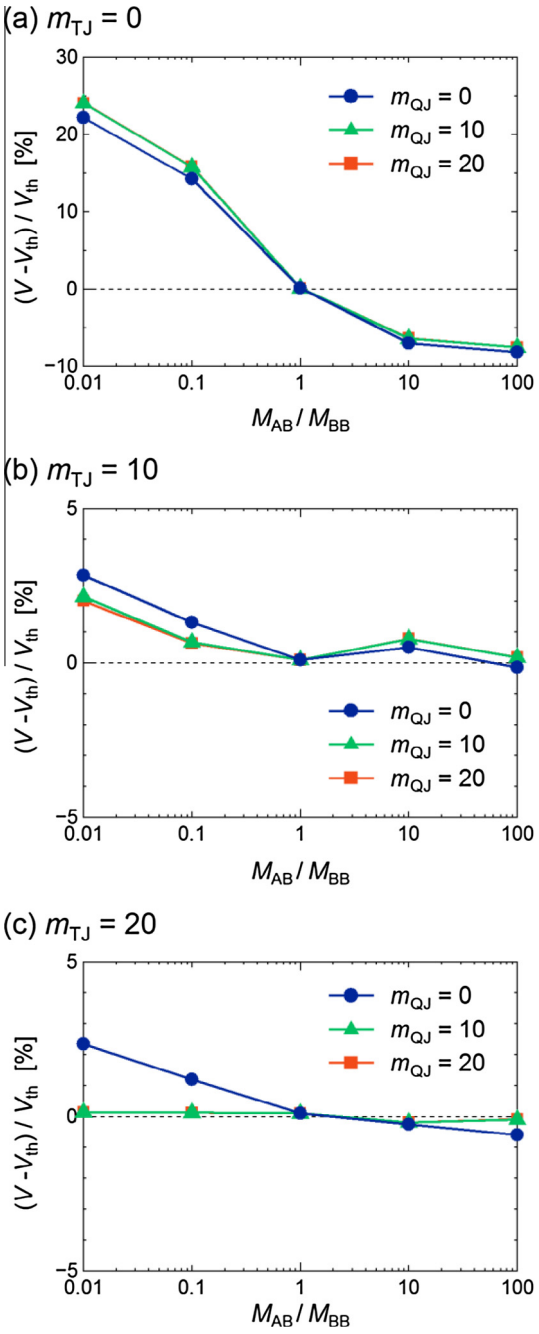

Fig. 6. Variation of $(V - V_{th})/V_{th}$ as a function of M_{AB}/M_{BB} for various m_{TJ} and m_{QJ} values.

Next, to confirm the validity of the extended higher-order MPF model with M_{ijk} (Eq. (9) with $m_{TJ} = 20$) and M_{ijkl} (Eq. (11) with $m_{QJ} = 20$), additional simulations were conducted in the same manner as described above. Here, the original model without higher-order-junction mobilities and the higher-order model with only M_{ijk} (Eq. (9) with $m_{TJ} = 20$) were also employed. The results are presented in Fig. 7. In contrast to the extended model, which yields results almost consistent with the theory, the original model and higher-order model with only M_{ijk} become inaccurate as M_{AB}/M_{BB} deviates from 1; the decrease in the accuracy is remarkable in the range of $M_{AB}/M_{BB} < 1$, and the errors reach several tens of percent. These findings indicate that the extended model is useful for handling the strongly anisotropic GB mobilities in 3D grain-growth simulations.

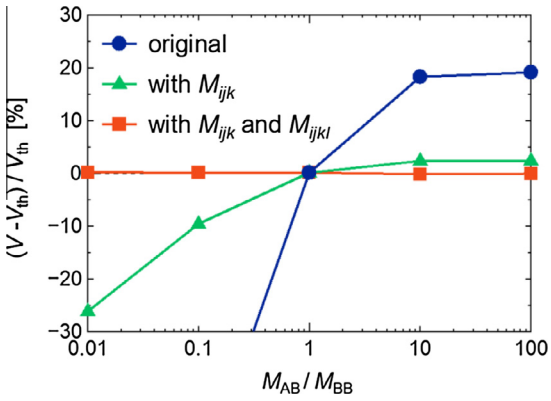

Fig. 7. Variation of $(V - V_{th})/V_{th}$ as a function of M_{AB}/M_{BB} obtained using three MPF models: the original model without higher-order-junction mobilities, higher-order model with only M_{ijk}, and extended higher-order model with M_{ijk} and M_{ijkl}.

3.3. Grain-growth simulations using misorientation-dependent GB properties

This section evaluates the accuracy of the extended higher-order MPF model, which uses the parameters determined in the previous sections, for the case where the GB energy and mobility are varied simultaneously. In this case, we also used the system shown in Fig. 1 as the simulation model. Here, the $\Delta\theta$-dependent GB energy, $\gamma(\Delta\theta)$, and mobility, $M(\Delta\theta)$, were introduced using the classical Read–Shockley model [63] and the sigmoidal model proposed by Humphreys [64], as follows:

$$\gamma(\Delta\theta) = \begin{cases} \gamma_m \frac{\Delta\theta}{\Delta\theta_m}\{1 - \ln\left(\frac{\Delta\theta}{\Delta\theta_m}\right)\} & \text{for } \Delta\theta \leqslant \Delta\theta_m, \\ \gamma_m & \text{for } \Delta\theta > \Delta\theta_m, \end{cases} \tag{15}$$

$$M(\Delta\theta) = \begin{cases} M_m\left[1 - \exp\{-5\left(\frac{\Delta\theta}{\Delta\theta_m}\right)^4\}\right] & \text{for } \Delta\theta \leqslant \Delta\theta_m, \\ M_m & \text{for } \Delta\theta > \Delta\theta_m, \end{cases} \tag{16}$$

where $\gamma_m = 1\ \mathrm{J/m^2}$, $M_m = 1\ \mathrm{m^4/(J\,s)}$, and $\Delta\theta_m = 15°$ are the energy, mobility, and minimum $\Delta\theta$ of the high-angle GBs, respectively.

Using Eqs. (15) and (16), simulations were performed with the $\Delta\theta$ of the A–B boundary, $\Delta\theta_{AB}$, and that of the B–B boundary, $\Delta\theta_{BB}$, varied up to $\Delta\theta_m = 15°$; the relative error $(V - V_{th})/V_{th}$ was calculated for each $\Delta\theta$ value. Here, either $\Delta\theta_{AB}$ or $\Delta\theta_{BB}$ was fixed to $\Delta\theta_m$, while the other was varied. Note that $\Delta\theta_{AB}$ must be limited within the range $\Delta\theta_{AB} \geqslant 4°$, which corresponds to the condition $\gamma_{BB}/\gamma_{AB} < \sqrt{3}$, to avoid solid-state wetting [60–62]. Fig. 8 shows the variations of $(V - V_{th})/V_{th}$ with $\Delta\theta$ calculated using three types of MPF models: the original model without higher-order-junction properties, higher-order model with only TJ properties, and extended higher-order model with TJ and QJ properties. As observed in Fig. 8(a), in the case of changing $\Delta\theta_{AB}$ with a constant $\Delta\theta_{BB}$, the error of the original model and higher-order model with TJ properties increases monotonically on the negative side as $\Delta\theta_{AB}$ decreases. Although the model with TJ properties is relatively accurate compared with the original model, the magnitude of the error becomes almost 20% at $\Delta\theta_{AB} = 4°$. However, the extended model with TJ and QJ properties maintains the accuracy with an error of less than approximately 1% for all the $\Delta\theta_{AB}$ values at which solid-state wetting does not occur. As demonstrated in Fig. 8(b), in the case of changing $\Delta\theta_{BB}$ with a constant $\Delta\theta_{AB}$, $(V - V_{th})/V_{th}$ of the original model increases monotonically with decreasing $\Delta\theta_{BB}$ and exceeds 10% at $\Delta\theta_{BB} = 9°$. The model with TJ properties maintains a high accuracy in the range $\Delta\theta_{BB} \geqslant 7°$ with an error of less than 2% in the negative side. However, for $\Delta\theta_{BB} < 7°$, the error suddenly jumps to the positive side and reaches 10% at

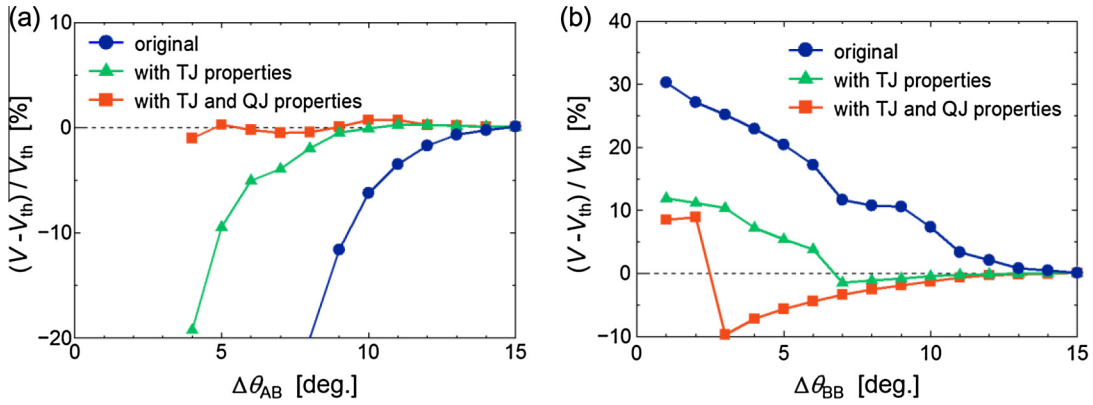

Fig. 8. Variation of $(V - V_{th})/V_{th}$ as a function of (a) $\Delta\theta_{AB}$ ($\Delta\theta_{BB} = 15°$) and (b) $\Delta\theta_{BB}$ ($\Delta\theta_{AB} = 15°$) for the anisotropic-grain-growth simulations using Eqs. (15) and (16). The results were obtained using three MPF models: the original model without higher-order-junction properties, higher-order model with only TJ properties, and extended higher-order model with TJ and QJ properties.

$\Delta\theta_{BB} = 4°$. Note that in the simulations performed using these models, a significant degree of ghost phases was observed for $\Delta\theta_{BB} < 7°$; this phenomenon can cause severe problems when simulating grain growth in more general systems. In contrast, the extended model allows for stable computation without the occurrence of ghost phases in the range $\Delta\theta_{BB} \geqslant 3°$. Although the error increases monotonically on the negative side, reaching almost 10% at $\Delta\theta_{BB} = 3°$, the accuracy is much higher than that of the original model.

The results summarized above confirm that the introduction of the QJ properties improves the accuracy of 3D MPF simulations with $\Delta\theta$-dependent GB properties. In particular, for $\Delta\theta_{BB} \geqslant 3°$, stable and accurate simulations can be performed with an error of less than 10% while preventing the formation of ghost phases.

4. Conclusions

This study was performed to improve the accuracy of 3D MPF grain-growth simulations using anisotropic GB energy and mobility. In this regard, the higher-order MPF model proposed in our previous study was extended to account for the properties of QJs. Further, the extended model was validated based on a series of anisotropic-grain-growth simulations. The main findings are summarized as follows:

(1) In cases where low-energy GBs migrate toward high-energy GBs, the error of 3D MPF simulations can be suppressed to approximately zero by introducing the higher-order term representing the free energy of QJs. However, in cases where high-energy GBs migrate toward low-energy GBs, the accuracy cannot be improved. If the accuracy improvement is needed for such cases, the MPF model must be modified by a method other than introducing higher-order terms.
(2) The introduction of the QJ mobility enables strongly anisotropic GB mobilities to be handled with a quite-high degree of accuracy in 3D MPF simulations.
(3) When $\Delta\theta$-dependent GB energy and mobility are introduced using the Read–Shockley model and the sigmoidal model proposed by Humphreys, the extended higher-order model can perform stable and accurate 3D simulations for the range of $\Delta\theta \geqslant 3°$, whereas the models without QJ properties become unstable for $\Delta\theta < 7°$.

To investigate the fundamental points that required modifications in the MPF modeling, this study focused on curvature-driven grain-growth simulations. Such simulations are essential for studying the fundamental nature of grain growth. However, from a practical viewpoint, it is important to consider additional factors in grain-growth simulations that were not discussed in the current study, including dispersed second-phase particles, chemical driving forces, and multiple phase transformations. We plan to address the validity of the present model for such applications in our future work. In addition, this study examined the appropriate modeling of the QJ properties, W_{ijkl} and M_{ijkl}, for the case of $\delta = 4\Delta x$. Kim et al. [65] have also reported that the condition $\delta = 4\Delta x$ is a good compromise between computational accuracy and cost in simulating curvature-driven 3D grain growth. However, when an additional driving force other than the grain-boundary curvature is considered, a larger value of δ could be required. Thus, if necessary, our future work will reformulate W_{ijkl} and M_{ijkl} so as to be applicable to any δ value.

References

[1] F.J. Humphreys, M. Hatherly, Recrystallization and Related Annealing Phenomena, second ed., Pergamon press, Oxford, 2004.
[2] D. Raabe, F. Roters, F. Barlat, L.-Q. Chen, Continuum Scale Simulation of Engineering Materials, Wiley-VCH, Weinheim, 2004.
[3] M.A. Miodownik, J. Light Met. 2 (2002) 125.
[4] A. Ayad, F. Wagner, N. Rouag, A.D. Rollett, Comput. Mater. Sci. 68 (2013) 189.
[5] A.D. Rollett, D.J. Srolovitz, M.P. Anderson, Acta Metall. 37 (1989) 1227.
[6] Y. Saito, M. Enomoto, ISIJ Int. 32 (1992) 267.
[7] D.J. Srolovitz, G.S. Grest, M.P. Anderson, Acta Metall. 34 (1986) 1833.
[8] H.W. Hesselbarth, I.R. Göbel, Acta Metall. Mater. 39 (1991) 2135.
[9] J. Geiger, A. Roósz, P. Barkóczy, Acta Mater. 49 (2001) 623.
[10] K.G.F. Janssens, Math. Comput. Simul. 80 (2010) 1361.
[11] K. Fuchizaki, K. Kawasaki, Mater. Sci. Forum 204–206 (1996) 267.
[12] D. Weygand, Y. Brechett, J. Lépinoux, Philos. Mag. B 80 (2009) 1987.
[13] K. Piękoś, J. Tarasiuk, K. Wierzbanowski, B. Bacroix, Comput. Mater. Sci. 42 (2008) 584.
[14] A. Vondrous, M. Reichardt, B. Nestler, Model. Simul. Mater. Sci. Eng. 22 (2014) 025014.
[15] F. Wakai, N. Enomoto, H. Ogawa, Acta Mater. 48 (2000) 1297.
[16] H.J. Frost, C.V. Thompson, C.L. Howe, J. Whang, Scr. Metall. 22 (1988) 65.
[17] E.A. Lazar, J.K. Mason, R.D. MacPherson, D.J. Srolovitz, Acta Mater. 59 (2011) 6837.
[18] E.A. Lazar, R.D. MacPherson, D.J. Srolovitz, Acta Mater. 58 (2010) 364.
[19] H. Hallberg, Model. Simul. Mater. Sci. Eng. 22 (2014) 085005.
[20] Y. Jin, N. Bozzolo, A.D. Rollett, M. Bernacki, Comput. Mater. Sci. 104 (2015) 108.
[21] L.-Q. Chen, Annu. Rev. Mater. Res. 32 (2002) 113.
[22] I. Steinbach, Model. Simul. Mater. Sci. Eng. 17 (2009) 073001.
[23] T. Takaki, A. Yamanaka, Y. Tomita, Adv. Struct. Mater. 64 (2015) 441.
[24] T. Takaki, Y. Tomita, Int. J. Mech. Sci. 52 (2010) 320.
[25] Y. Suwa, Nippon Steel Tech. Rep. 102 (2013) 19.
[26] I. Steinbach, F. Pezzolla, Physica D 134 (1999) 385.
[27] I. Steinbach, F. Pezzolla, B. Nestler, M. Seeßelberg, R. Prieler, G.J. Schmitz, J.L.L. Rezende, Physica D 94 (1996) 135.
[28] S. Vedantam, B.S.V. Patnaik, Phys. Rev. E 73 (2006) 016703.
[29] T. Takaki, T. Hirouchi, Y. Hisakuni, A. Yamanaka, Y. Tomita, Mater. Trans. 49 (2008) 2559.
[30] M. Ohno, S. Tsuchiya, K. Matsuura, Acta Mater. 59 (2011) 5700.

[31] J. Gruber, N. Ma, Y. Wang, A.D. Rollett, G.S. Rohrer, Model. Simul. Mater. Sci. Eng. 14 (2006) 1189.
[32] S.G. Kim, D.I. Kim, W.T. Kim, Y.B. Park, Phys. Rev. E 74 (2006) 061605.
[33] G. Gottstein, L.S. Shvindlerman, Grain Boundary Migration in Metals: Thermodynamics, Kinetics, Applications, CRC Press, Boca Raton, 1999.
[34] Y. Shibuta, S. Takamoto, T. Suzuki, Comput. Mater. Sci. 44 (2009) 1025.
[35] Y. Shibuta, S. Takamoto, T. Suzuki, ISIJ Int. 48 (2008) 1582.
[36] M. Upmanyu, G.N. Hassold, A. Kazaryan, E.A. Holm, Y. Wang, B. Patton, D.J. Srolovitz, Interface Sci. 10 (2002) 201.
[37] E.A. Holm, M.A. Miodownik, A.D. Rollett, Acta Mater. 51 (2003) 2701.
[38] A. Kazaryan, Y. Wang, S.A. Dregia, B.R. Patton, Acta Mater. 50 (2002) 2491.
[39] A.D. Rollett, JOM 56 (2004) 63.
[40] Y. Suwa, Y. Saito, H. Onodera, Comput. Mater. Sci. 40 (2007) 40.
[41] N. Moelans, F. Wendler, B. Nestler, Comput. Mater. Sci. 46 (2009) 479.
[42] H. Garcke, B. Nestler, B. Stoth, SIAM, J. Appl. Math. 60 (1999) 295.
[43] B. Nestler, H. Garcke, B. Stinner, Phys. Rev. E 71 (2005).
[44] T. Hirouchi, T. Tsuru, Y. Shibutani, Comput. Mater. Sci. 53 (2012) 474.
[45] E. Miyoshi, T. Takaki, Comput. Mater. Sci. 112 (2016) 44.
[46] M. Hillert, Acta Metall. 13 (1965) 227.
[47] Y. Suwa, Y. Saito, H. Onodera, Mater. Trans. 49 (2008) 704.
[48] A. Vondrous, P. Bienger, S. Schreijäg, M. Selzer, D. Schneider, B. Nestler, D. Helm, R. Mönig, Comput. Mech. 55 (2015) 439.
[49] A. Vondrous, M. Selzer, J. Hotzer, B. Nestler, Int. J. High Perform. Comput. Appl. 28 (2013) 61.
[50] S. Sakane, T. Takaki, M. Ohno, T. Shimokawabe, IOP Conf. Ser. Mater. Sci. Eng. 84 (2015) 012063.
[51] T. Takaki, R. Rojas, M. Ohno, T. Shimokawabe, T. Aoki, IOP Conf. Ser. Mater. Sci. Eng. 84 (2015) 012066.
[52] A. Yamanaka, T. Aoki, S. Ogawa, T. Takaki, J. Cryst. Growth 318 (2011) 40.
[53] M. Okamoto, A. Yamanaka, T. Shimokawabe, T. Aoki, Trans. Jpn. Soc. Comput. Eng. Sci. 2013 (2013) 20130018.
[54] T. Takaki, T. Shimokawabe, M. Ohno, A. Yamanaka, T. Aoki, J. Cryst. Growth 382 (2013) 21.
[55] T. Takaki, M. Ohno, T. Shimokawabe, T. Aoki, Acta Mater. 81 (2014) 272.
[56] Y. Shibuta, M. Ohno, T. Takaki, JOM 67 (2015) 1793.
[57] T. Takaki, M. Ohno, Y. Shibuta, S. Sakane, T. Shimokawabe, T. Aoki, J. Cryst. Growth 442 (2016) 14.
[58] T. Takaki, T. Hirouchi, Y. Tomita, J. Cryst. Growth 310 (2008) 2248.
[59] M. Ohno, K. Matsuura, Acta Mater. 58 (2010) 6134.
[60] H. Park, J. Appl. Phys. 95 (2004) 5515.
[61] K. Ko, P. Cha, D.J. Srolovitz, N. Hwang, Acta Mater. 57 (2009) 838.
[62] W. Guo, I. Steinbach, Int. J. Mater. Res. 101 (2010) 480.
[63] W.T. Read, W. Shockley, Phys. Rev. 78 (1950) 275.
[64] F.J. Humphreys, Acta Mater. 45 (1997) 4231.
[65] H.-K. Kim, S.G. Kim, W. Dong, I. Steinbach, B.-J. Lee, Model. Simul. Mater. Sci. Eng. 22 (2014) 034004.